UC Merced

UC Merced Previously Published Works

Title

Origin of Pressure-Dependent Adhesion in Nanoscale Contacts

Permalink

https://escholarship.org/uc/item/3sw4m1ts

Journal

Nano Letters, 22(14)

ISSN

1530-6984

Authors

Baker, Andrew J
Vishnubhotla, Sai Bharadwaj
Chen, Rimei
et al.

Publication Date

2022-07-27

DOI

10.1021/acs.nanolett.2c02016

Peer reviewed

eScholarship.org Powered by the California Digital Library
University of California

NANO LETTERS

pubs.acs.org/NanoLett

Letter

Origin of Pressure-Dependent Adhesion in Nanoscale Contacts

Andrew J. Baker, Sai Bharadwaj Vishnubhotla, Rimei Chen, Ashlie Martini, and Tevis D. B. Jacobs*

Cite This: *Nano Lett.* 2022, 22, 5954−5960

Read Online

ACCESS | Metrics & More | Article Recommendations | Supporting Information

ABSTRACT: The adhesion between nanoscale components has been shown to increase with applied load, contradicting well-established mechanics models. Here, we use *in situ* transmission electron microscopy and atomistic simulations to reveal the underlying mechanism for this increase as a change in the mode of separation. Analyzing 135 nanoscale adhesion tests on technologically relevant materials of anatase TiO_2, silicon, and diamond, we demonstrate a transition from fracture-controlled to strength-controlled separation. When fracture models are incorrectly applied, they yield a 7-fold increase in *apparent* work of adhesion; however, we show that the *true* work of adhesion is unchanged with loading. Instead, the nanoscale adhesion is governed by the product of adhesive strength and contact area; the pressure dependence of adhesion arises because contact area increases with applied load. By revealing the mechanism of separation for loaded nanoscale contacts, these findings provide guidance for tailoring adhesion in applications from nanoprobe-based manufacturing to nanoparticle catalysts.

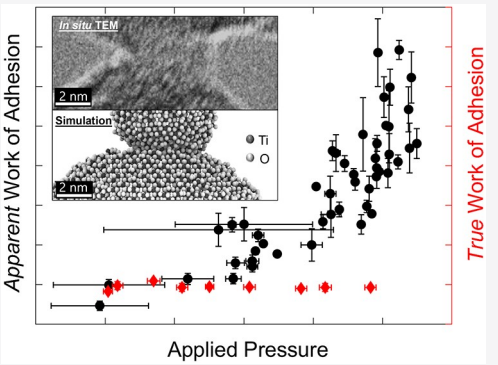

KEYWORDS: *Work of adhesion, Nanoscale contacts, Fracture-controlled separation, Strength-controlled decohesion, In situ TEM, Molecular dynamics simulation*

Nanoscale adhesion governs the performance of small-scale technologies, including nanomanufacturing,[1] scanning-probe microscopy and metrology,[2] and nanodevices.[3] It is also relevant for large-scale components as the properties of macroscopic surfaces are governed by their nanoscale features due to surface roughness.[4] For decades, the adhesion of nanoscale components has been characterized primarily using continuum-mechanics models for elastic[5−8] and elastic−plastic contacts.[9,10] In fact, this process, measuring adhesion using an atomic force microscope and analyzing the data using continuum mechanics models, remains the state-of-the-art method for measuring adhesion energy.[11−13] These contact-mechanics models describe the separation of the contacting interface using fracture mechanics,[14] assuming a sphere of radius R on a flat substrate with a certain work of adhesion W_{adh} between the two materials. In these models,[8] the force of adhesion F_{adh} is described by

$$F_{adh} = \alpha\pi R W_{adh} \quad (1)$$

where the value of the constant α ranges from 1.5 to 2, as determined by the Maugis parameter[8,15] of the contact.

However, recent work has demonstrated that the adhesion force can be dependent on applied load.[16−19] One possible explanation for this is an increase in interfacial work of adhesion with loading, as a result of the formation of chemical bonds across the interface. These load-induced changes in interfacial bonding are well-supported by investigations measuring adhesion and friction,[20−22] and simulations examining the number of bonds as a function of load and time.[20,23−24] In a prior investigation of loaded nanocontacts by the present authors, the work of adhesion computed using eq 1 was shown to increase 7-fold with applied pressure,[19] reaching a maximum value over 7 J/m^2; however, the fundamental origin of this increasing adhesion has not yet been identified. The purpose of the present investigation is to determine the origin of load-dependent nanoscale adhesion, through the comprehensive analysis of nanoscale adhesion tests performed with *in situ* transmission electron microscopy (TEM) coupled with molecular dynamics (MD) simulations. The goal is to disentangle effects of interfacial chemistry from those of morphological changes in the contacting bodies.

In the present investigation, nanoscale adhesion tests were performed (see Experimental Methods) on a self-mated contact of anatase TiO_2 inside of a TEM, as shown in Figure 1a. This experimental apparatus provides simultaneous measurement of nanonewton-scale forces and angstrom-scale morphology and structure. The material was chosen as TiO_2 for two reasons: first, technologically, it is an important material for photocatalysts and photovoltaics,[25] where nanoscale adhesion is a critical parameter for performance;[26] and second, scientifically, it provides a self-mated crystalline oxide

Received: May 18, 2022
Revised: June 30, 2022
Published: July 6, 2022

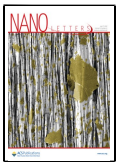

ACS Publications

© 2022 The Authors. Published by American Chemical Society

https://doi.org/10.1021/acs.nanolett.2c02016
Nano Lett. 2022, 22, 5954−5960

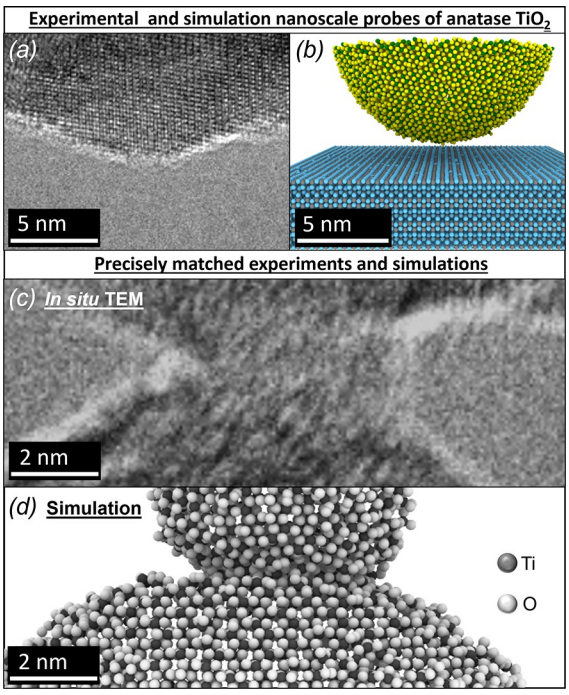

Figure 1. The load-dependence of nanoscale adhesion was investigated for anatase TiO_2, using *in situ* TEM (a) and molecular dynamics simulations (b). Simulations were conducted on hemispheres (b), as well as shapes that were precisely matched to experimental probes. Real-time in-contact images are shown for the matched probes in panels c and d.

system, which is simpler to understand than prior investigations of dissimilar interfaces, such as the previous work[19] on silicon (potentially containing an amorphous native oxide) and carbon (which can take various hybridization states). MD simulations were also carried out (Figure 1b), to gain atomic-level insights into the contact behavior of the same material (see Simulation Methods). Various contact geometries were modeled including spheres, flat punches, and a geometry that was precisely matched to one of the *in situ* experimental samples (Figure 1c,d).

The experimental and simulation data for TiO_2 was first analyzed using the conventional contact-mechanics models discussed above (eq 1). Specifically, we used an implementation[15] of the Maugis-Dugdale model,[8] as described in detail in ref 19. This fracture-based analysis of the data (Figure 2a) concludes that the apparent work of adhesion increases with applied pressure from 1 J/m^2 at light loads to approximately 7 J/m^2 at high loads. Remarkably, this behavior is nearly identical to the previously reported[19] behavior of silicon in contact with diamond (replotted here in Figure 2b).

The application of these conventional models is undermined by an analysis of the mechanism of separation, that is, accounting for the transition from fracture-controlled (cracklike) separation to strength-controlled (uniform) separation.[27−30] This type of analysis has been extensively investigated in soft materials[31] and is often discussed in terms of "flaw sensitivity"[32] "load sharing"[33] or "uniform and non-uniform bond breaking".[34,35] Conventional adhesion models, such as those of JKR[6] or Maugis,[8] apply only to the fracture-controlled limit and describe a Griffith-like balance between the energy of the interface (e.g., the chemical energy of the interfacial atomic bonds) and the stored energy in the material (i.e., the elastic mechanical energy of the deformed body). When the gradient of energy versus crack length is negative, then the crack becomes unstable and the contact separates. These conventional models do not apply in the strength-controlled limit, where separation is uniform (rather than cracklike). For flat punches, the transition between these limits depends on the size of the punch.[27,28] There is a critical radius defined by $r_{crit} = 8E^*W_{adh}/\pi\sigma_{adh}^2$, where σ_{adh} is the adhesive strength and E^* is the effective modulus (given by $E^* = [(1-\upsilon_1^2)/E_1 + (1-\upsilon_2^2)/E_2]^{-1}$, where 1 and 2 designate the two materials in contact). Above this critical radius, fracture mechanics applies; below this radius, fracture mechanics does not apply. In the latter regime, the separation occurs uniformly, and the adhesive force is described by

$$F_{adh} = A_{cont}\sigma_{adh} \tag{2}$$

where A_{cont} is the area of contact (or the area of interaction if adhesive forces extend beyond the boundaries of the contact).

Describing the separation process of spheres is slightly more complicated because the contact size is not constant but rather varies with load. This behavior has been described previously for both elastic spheres[30] and plastic spheres.[29] The latter model is especially useful for larger loads or high-adhesion contacts, where plasticity is expected to play a role. In that model, the loading behavior is assumed to be plastic, while the unloading behavior may be elastic or plastic depending on the physical interactions. The behavior during separation is governed by two dimensionless parameters. First, a material-dependent parameter S determines whether the separation behavior is primarily elastic or plastic

$$S = \frac{\sigma_{adh}}{H} \tag{3}$$

by comparing the adhesive strength to the hardness H of the softer material. Second, a material- and geometry-dependent parameter χ describes the ratio of adhesion energy to stored elastic energy in the plastically deformed contact

$$\chi = \frac{\pi}{2\pi - 4}\frac{W_{adh}E^*}{H^2 a_{cont}} \tag{4}$$

where a_{cont} is the contact radius. Lower values of χ indicate weaker adhesion and/or larger amounts of stored elastic energy and will tend to separate via a fracturelike process. Higher values of χ (strong adhesion and/or less stored elastic energy) will tend to separate by uniform separation. The critical value where this transition in adhesive behavior occurs, designated χ_{crit}, is dependent on the value of S, as described in ref 29.

In the present analysis of nanoscale adhesion in TiO_2 and silicon-diamond contacts, Johnson's model was applied in a self-consistent way using the minimum possible number of assumptions (described below, with more details in Supporting Information Analysis of Separation Mechanism). Specifically, the application of Johnson's model to each material system required knowledge of four material parameters: hardness H, work of adhesion W_{adh}, adhesive strength σ_{adh}, and effective modulus E^*. Three of the four parameters were extracted directly from the experimental measurements; only the modulus of the materials was taken from prior literature, which is justified because the elastic modulus of materials is dependent on fundamental atomic bonding interactions and is not generally considered to be strongly size-dependent.[36] Once

https://doi.org/10.1021/acs.nanolett.2c02016
Nano Lett. 2022, 22, 5954−5960

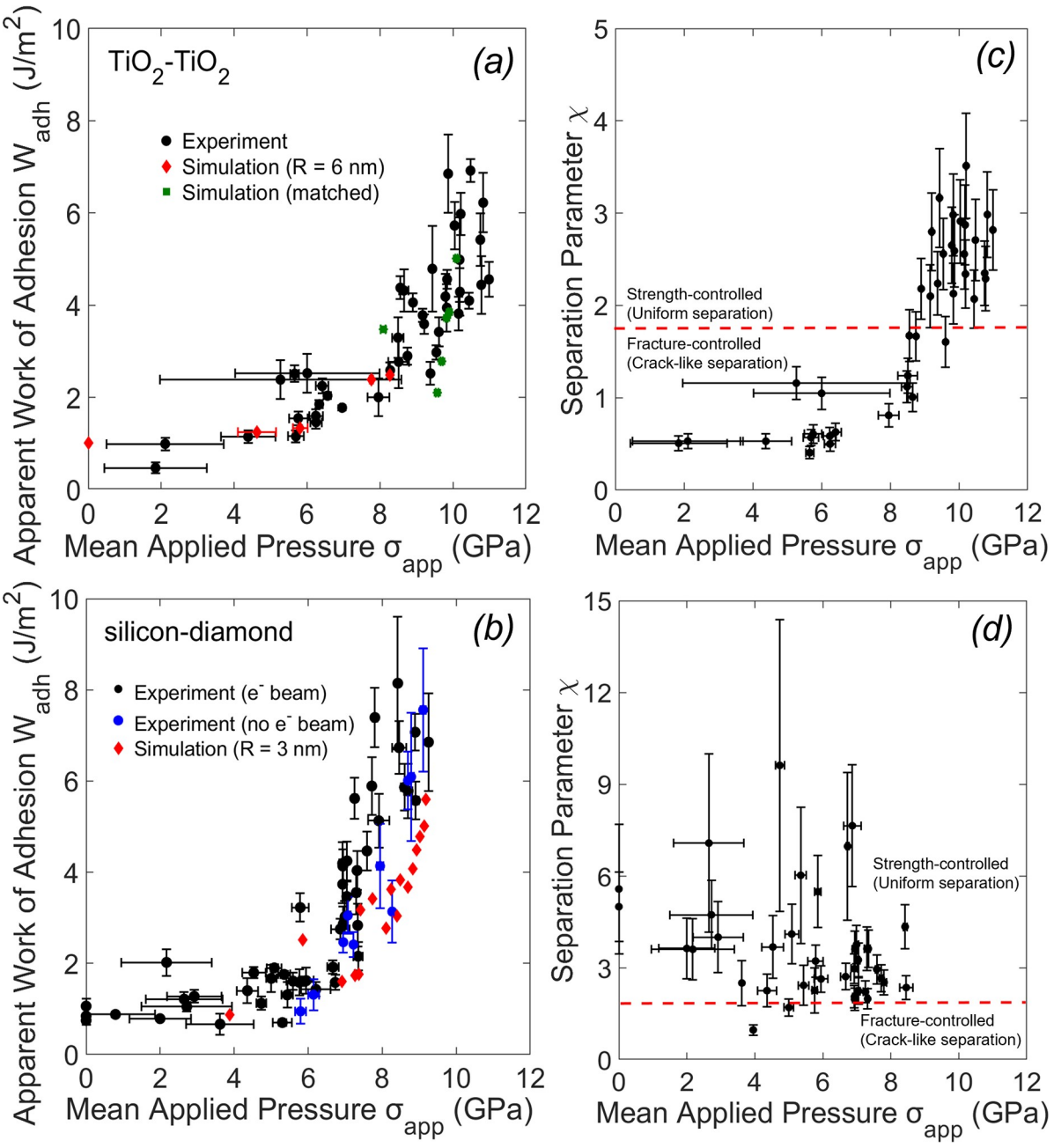

Figure 2. Apparent trends of increasing work of adhesion are compelling but ultimately misleading. When the data is analyzed using conventional (fracture-based) models (eq 1), the apparent work of adhesion seems to be strongly pressure-dependent for these nanoscale contacts of TiO_2−TiO_2 (a) and silicon-diamond (b). Note that two types of simulations are included: hemispherical probes with radius R designated in the legend (red diamonds) and a model probe (green squares) with shape and size matched to that in an experiment (see Figure 1). When the data is reanalyzed (c and d) to account for the separation mechanism (fracture-controlled versus strength-controlled, see main text), it is shown that most of the data should instead be analyzed in the context of strength-controlled separation (eq 2).

these values are determined, then a specific value of χ can be computed for each contact using eq 4 and a measurement of a_{cont} from the *in situ* TEM video.

When the data in Figure 2a,b are analyzed in the context of the mechanism of separation, the results reveal that most of the nanoscale adhesion tests lie in the strength-controlled limit (Figure 2c,d). Therefore, the commonly used fracture-based models do not apply. Specifically, for TiO_2−TiO_2 contacts χ_{crit} = 1.87 ± 0.25 with S = 0.96 ± 0.05 and for silicon−diamond χ_{crit} = 1.90 ± 0.34 with S = 0.97 ± 0.07. The very lowest-load tests on anatase TiO_2 fall in the fracture-controlled limit and give a consistent value for work of adhesion of 0.87 ± 0.15 J/m^2. However, as the pressure increases, the value of the flaw-sensitivity parameter χ increases, eventually exceeding χ_{crit}. Likewise, almost all of the adhesion measurements of silicon on diamond lie in the regime where $\chi > \chi_{crit}$, implying that fracture-based models (used in Figure 2b) should not be used.

Considering this result, these nanoscale adhesion values must be reinterpreted, accounting for their strength-limited behavior. Therefore, we have determined the instantaneous contact area during each test, for both experimental and simulated contacts (Figure 3a) and plotted the adhesive force

https://doi.org/10.1021/acs.nanolett.2c02016
Nano Lett. 2022, 22, 5954−5960

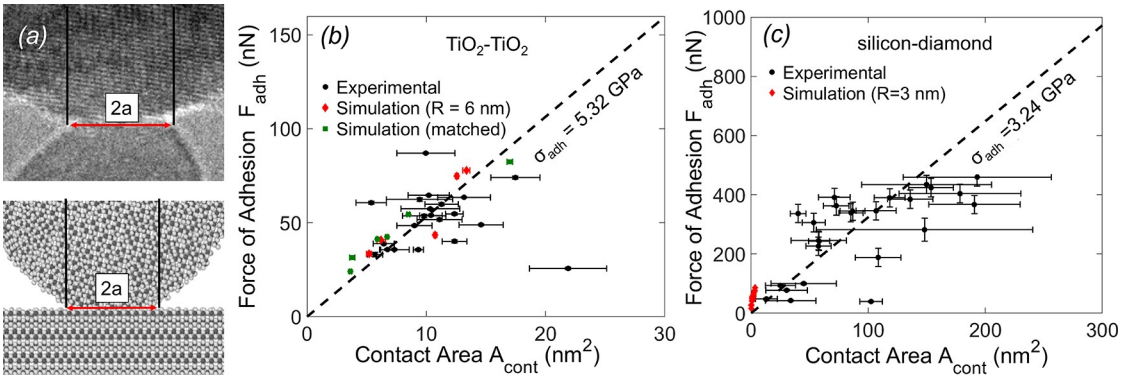

Figure 3. The previously observed increase in apparent work of adhesion is found to correspond to strength-controlled separation, with the load-dependent increase in pull-off force arising from changes in the contact size. To account for strength-limited separation, all contact tests where $\chi > \chi_{crit}$ are plotted with pull-off force as a function of measured contact area from experiments and simulations (a). The results for TiO_2−TiO_2 (b) and silicon−diamond (c) show that the measured increase in pull-off forces is primarily attributable to an increase in contact area with increasing load, rather than due to changes in chemistry at the interface. Some of the data in (c) was collected with a higher-vibration tester, so data points with uncertainty >75% of the measured value have been omitted for clear visualization; the full data are included in Figure S3. The dashed lines in (b,c) show $F_{adh} = A_{cont}\sigma_{adh}$, where the value of σ_{adh} is the average value of F_{adh}/A_{cont}.

against this contact area for all tests where $\chi > \chi_{crit}$ (Figure 3b,c). The results show proportional behavior in all cases, demonstrating the applicability of a strength-controlled description. For the high-χ contacts of TiO_2, the adhesive strength is found to be 5.32 ± 0.30 GPa with no statistically significant difference between the experimental and simulated results (95% confidence). Additionally, we have reanalyzed our prior tests of silicon on diamond accounting for the mechanism of separation. The adhesive strength measured from silicon−diamond was 3.24 ± 0.24 GPa. We note that those prior experimental tests were performed on a higher-vibration tester (see Supporting Information Detailed Experimental Methods); for clarity, the measurements with highest uncertainty are omitted from Figure 3c and are shown in Figure S3. Additionally, the experiments and simulations in this prior testing cover different ranges of contact sizes, complicating the direct comparison of results. However, the overall trend of increasing force of adhesion with increasing contact area supports the present interpretation.

To further understand the atomic-scale significance of these results, atomistic simulations were performed on flat-punch contacts of the TiO_2 material (Simulation Methods). In these simulations, flat blocks of this material were brought into contact and loaded up to various maximum loads before separation (Figure 4a), such that the mean applied pressure ranged from 0 to 10 GPa (approximately equal to the hardness of the material). To understand the nature of bonding at the interface, the work of adhesion can be computed directly using its definition. To do this, we calculated the energy difference (per unit area) between the surfaces in contact at zero applied load (just before separation) and the surfaces after separation $(E_{apart} - E_{cont})/A_{cont}$. The simulations demonstrate that the work of adhesion does not increase with applied load for a flat-punch contact (Figure 4b). The resulting work of adhesion for the flat-punch TiO_2 contact is 0.95 ± 0.02 J/m^2. This calculated value is consistent (95% confidence) with the work of adhesion determined above (0.87 ± 0.15 J/m^2), computed by analyzing only the very lowest-load sphere-flat tests using eq 1, (i.e., applied to low-χ tests that separated in a fracture-controlled manner). Additionally, the adhesive strength (Figure 4c) can be calculated from the adhesive force of the flat-punch contacts using eq 2, yielding a value of 5.54 ± 0.1

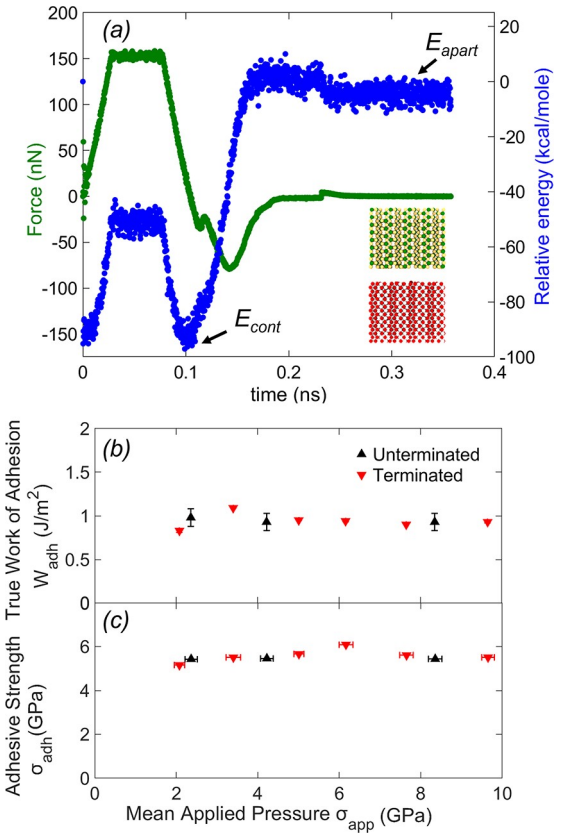

Figure 4. Flat-punch simulations reveal that the true work of adhesion does not vary with increasing applied pressure. Loading-and-adhesion simulations were performed on anatase TiO_2 (unterminated and hydrogen-terminated), loaded to various levels of maximum force while tracking the instantaneous force and energy in the simulation (a). The work of adhesion is measured using its definition and is shown to be approximately constant at 0.95 J/m^2 for all values of applied pressure (b). Finally, the adhesive strength, as measured for strength-limited separation, is shown in panel (c) and also does not change with increasing pressures.

GPa, which is not significantly different (95% confidence) from the value computed from the sphere-flat tests in Figure 3b (5.32 ± 0.30 GPa). The value of adhesive strength does not

https://doi.org/10.1021/acs.nanolett.2c02016
Nano Lett. 2022, 22, 5954−5960

change with increasing applied pressure for either H-terminated or unterminated surfaces, showing that there are no significant load-dependent changes in the strength of interaction at the interface.

These findings provide conclusive evidence for the origin of load-dependent adhesion in these loaded nanocontacts. Our prior work[19] had shown an increase in "apparent" work of adhesion between silicon and diamond up to approximately 7 J/m^2. Various explanations were considered including extreme increases in interfacial bonding, or possibly energy dissipation due to near-surface plasticity during separation. However, the present results demonstrate that the high apparent work of adhesion arises not from physical changes to the interface but rather from a misapplication of a fracture-based model in a case of strength-limited separation. The self-mated anatase TiO_2 showed a similar 7-fold increase in apparent work of adhesion, yet the true value of work of adhesion is far lower (0.95 J/m^2) and is insensitive to load over the tested range. Instead, it is the contact area between the two bodies that increases with load which, when coupled with a constant adhesive strength, yields a proportional increase in adhesive force.

These results shed new light on the physics of separation in nanoscale contacts. They challenge the common understanding of nanoscale adhesion as governed by a fracture-based process that obeys a Griffith energy balance, and which can be described using the very simple eq 1. Instead of these models, the contact and separation behavior will depend on the materials and geometry in contact. For elastic contact at the lightest loads between low-adhesion materials, fracture-based models will likely apply as typically used (eq 1). However, in highly adhesive materials (where $S > 1$), Johnson's model predicts that such models will never apply, regardless of how small the applied load. In materials that are stiffer or have lower adhesion ($S < 1$), the material parameter χ must be computed, preferably from direct or indirect measurements of contact area (rather than based on predictions of contact models). In cases where $\chi > \chi_{crit}$, the behavior is described by uniform strength-limited separation, and the force of adhesion is described by eq 2. Even in cases where $\chi < \chi_{crit}$, and the conventional fracture based models[8] are expected to apply, one cannot expect to get the correct value of work of adhesion using a measurement of tip radius before the test was performed. The explanation for this is that the tip shape may change significantly during loading, such that the separation behavior is governed by a new tip radius that is determined by the amount of elastic recovery in the material after plastic deformation (what Johnson calls the "elastically recovered crown").[29]

It is useful to use the Johnson model to estimate how the results would change for other materials with very different material properties. For instance, in a low-hardness material (which can be approximated by reducing H by a factor of 10 and keeping other material parameters constant), the computed values would be $S = 9.57$ and $\chi_{crit} = 2$. In this case, a contact radius larger than 288 nm would be expected to separate by fracture (eq 1) and a smaller contact radius by uniform pop-off (eq 2). On the other hand, in a weakly adhering material (which can be approximated by reducing W_{adh} and σ_{adh} by a factor of 10 while keeping other material parameters constant), the computed values would be $S = 0.10$ and $\chi_{crit} = 0.11$. Here, a contact radius smaller than 5.5 nm would be expected to separate by uniform pop-off. However, we note that the predictions in this paragraph depend on the accuracy of the Johnson model; the rest of the findings in this paper are consistent with the Johnson model but do not depend on its correctness.

The importance of plasticity and the increase in contact area in loaded nanocontacts was not previously recognized because the shapes of the bodies did not typically change appreciably. It was previously shown,[19] through pre- and post-test TEM imaging, that there was no significant shape change in the parabolic tip due to testing, which was also confirmed in the present work (Supporting Information Section S3). While the lack of shape change was previously assumed to indicate a lack of plastic deformation, it can instead be explained by the "elastically recovered crown" (mentioned in the prior paragraph),[29] which may result in a certain tip radius even after significant plastic deformation. The lack of evidence of dislocations or other plasticity mechanisms in the tip after contact (Supporting Information Figure S3) can be explained by previous results showing how defects can exit a nanoscale component upon unloading.[37]

There are numerous examples in the literature where contact-mechanics models can be accurately fit to measured results of adhesion, friction, or electrical current (see ref 38 for a review). In some cases, the adhesion may be low enough or the tip large enough that $\chi < \chi_{crit}$, and so fracture-based models would be appropriate. In other cases, including the prior investigation into silicon on diamond,[17] the fit may be almost incidental, arising due to the qualitatively similar behavior of different separation models. For example, in ref 17 achieving a fit between the data and the model required empirical variation of W_{adh} as a fitting parameter; this is equivalent to the analysis that is performed in Figure 2b, which is based on applying an inapplicable model.

On a practical level, this new understanding of nanoscale separation has important implications for materials characterization and for controlling adhesion in nanoscale devices. These findings challenge the most common method for measuring and reporting the strength of adhesion of an interface, which is to measure the pull-off force using an atomic force microscope and then apply simple contact-mechanics models (eq 1) to compute the work of adhesion. In many cases, this approach incorrectly describes the separation and yields incorrect results. In such cases, adhesion is governed by a process of uniform separation, and the interface should be characterized by its adhesion strength using eq 2. Furthermore, any attempt to tailor adhesion must correctly account for the mechanism of separation. A fracture-based understanding implies that adhesion is controlled only by the interfacial bonding. However, for strength-controlled separation, the adhesion of a nanoparticle or nanoprobe also depends on its area of contact, and therefore on the prior history of the amount of load previously applied.

In summary, we have combined *in situ* TEM adhesion testing and MD simulation of nanoscale contacts of technologically relevant materials. The results demonstrate that most of the contacts do not separate according to fracture mechanics, as previously believed, but instead separate in a uniform fashion. Although there was a 7-fold increase in "apparent" work of adhesion with increasing applied load, the true work of adhesion was shown to be constant and load-independent. Instead, the load-dependent adhesion is attributable to an increase in the contact area. This insight initiates a new paradigm for the characterization of interfacial adhesion

https://doi.org/10.1021/acs.nanolett.2c02016
Nano Lett. 2022, 22, 5954−5960

and suggests novel strategies for controlling the adhesion of nanoparticles and other small-scale devices.

EXPERIMENTAL METHODS

Adhesion testing was performed using an *in situ* TEM nanomanipulator (Biasing Manipulator Model 1800, Hummingbird Scientific, Lacey, WA) inside of a transmission electron microscope (Titan Themis G2 200, ThermoFisher Scientific, Waltham, MA). Contact was made between commercial silicon atomic force microscopy probes (PPP-NCLR, NCHR, FMR Nanosensors, Neuchatel, Switzerland) which had initial apex radii of approximately 5 nm and a plasma-cleaned silicon TEM wedge substrate (<200 nm Plateau, Bruker, Billerica, MA), with a plateau thickness of approximately 10 nm. Before testing, an approximately 30 nm layer of TiO_2 was deposited on the AFM probe and silicon TEM wedge (Angstrom Engineering NexDep Sputter Deposition Tool) and annealed at 550 °C for 2 h to form crystalline anatase. Additional tests were performed on TiO_2 nanoparticles (<25 nm, Sigma-Aldrich) that were drop-cast onto the silicon TEM wedge. The applied and adhesive force were determined by measuring the deflection of the calibrated cantilever, as described in ref 19. (Detailed Experimental Methods are provided in Supporting Information Section S1).

SIMULATION METHODS

Molecular dynamics simulations were performed on two different systems: (1) TiO_2 probe on TiO_2 block and (2) TiO_2 block on TiO_2 block. The model systems had periodic boundaries in the directions parallel to the surfaces of the blocks and fixed boundaries in the surface-normal directions. For the TiO_2 block on TiO_2 block, the dimensions were 3 nm × 3 nm × 3 nm for each block. For the TiO_2 probe on TiO_2 block, the block had dimensions of 15 nm × 15 nm × 4 nm. The probe was either a hemisphere with 6-nm radius, or an irregular shape designed to match the geometry of an experimental tip. The irregular shape was created by tracing the 2D profile from a TEM image and then creating a 3D solid using an approach we reported previously.[17] The bottommost 0.5 nm of atoms of the lower blocks were fixed in both models and the topmost 0.5 nm of atoms of the top probe or block were treated as a rigid body. Two variations of both TiO_2 models were created, either terminated with 100% hydrogen or unterminated. To simulate indentation, the upper body of each model was moved downward at 5 m/s until it reached approximately the desired maximum force. The upper body was held at this position until the potential energy reached steady state. Then, the upper body was moved upward at 5 m/s until the two bodies completely separated. During the simulation, the force was calculated as the sum of the forces on the atoms of the upper body. The simulations were run in the NVT ensemble (constant number of atoms, volume, and temperature) at 300 K. All simulations were performed using the large-scale atomic/molecular massively parallel simulator (LAMMPS).

ASSOCIATED CONTENT

Supporting Information

The Supporting Information is available free of charge at https://pubs.acs.org/doi/10.1021/acs.nanolett.2c02016.

Section S1, Detailed Experimental Methods, contains a description of the *in situ* adhesion testing, a description of the video of adhesion testing, and a description of analysis for contact size, adhesive force, and adhesive strength; Section S2, Analysis of Separation Mechanism, describes analysis of the separation mechanism (PDF)

Video of *in situ* TEM adhesion testing (MOV)

AUTHOR INFORMATION

Corresponding Author

Tevis D. B. Jacobs − *Department of Mechanical Engineering and Materials Science, University of Pittsburgh, Pittsburgh, Pennsylvania 15261, United States;* orcid.org/0000-0001-8576-914X; Email: tjacobs@pitt.edu

Authors

Andrew J. Baker − *Department of Mechanical Engineering and Materials Science, University of Pittsburgh, Pittsburgh, Pennsylvania 15261, United States;* orcid.org/0000-0002-4842-561X

Sai Bharadwaj Vishnubhotla − *Department of Mechanical Engineering and Materials Science, University of Pittsburgh, Pittsburgh, Pennsylvania 15261, United States;* orcid.org/0000-0002-4611-3313

Rimei Chen − *Department of Mechanical Engineering, University of California-Merced, Merced, California 95343, United States*

Ashlie Martini − *Department of Mechanical Engineering, University of California-Merced, Merced, California 95343, United States;* orcid.org/0000-0003-2017-6081

Complete contact information is available at: https://pubs.acs.org/10.1021/acs.nanolett.2c02016

Notes

The authors declare no competing financial interest.

The data that supports this publication has been deposited in an institutional repository and can be accessed using the following DOI: 10.18117/2vrk-ac47

ACKNOWLEDGMENTS

The authors gratefully acknowledge useful discussion with Prof. Lars Pastewka (U. Freiburg) about the results and analysis.The authors acknowledge support by the National Science Foundation (NSF) under Grants 1844739, 1536800, and 1537613. Use of the Nanoscale Fabrication & Characterization Facility in the Petersen Institute of Nanoscience and Engineering at the University of Pittsburgh (PINSE) is acknowledged.

REFERENCES

(1) Jiang, T.; Zhu, Y. Measuring Graphene Adhesion Using Atomic Force Microscopy with a Microsphere Tip. *Nanoscale* **2015**, *7*, 10760−10766.

(2) Deng, Z.; Smolyanitsky, A.; Li, Q.; Feng, X.; Cannara, R. J. Adhesion-Dependent Negative Friction Coefficient on Chemically Modified Graphite at the Nanoscale. *Nat. Mater.* **2012**, *11* (12), 1032.

(3) Loh, O. Y.; Espinosa, H. D. Nanoelectromechanical Contact Switches. *Nat. Nanotechnol.* **2012**, *7* (5), 283.

(4) Pastewka, L.; Robbins, M. O. Contact between Rough Surfaces and a Criterion for Macroscopic Adhesion. *Proc. Natl. Acad. Sci. U. S. A.* **2014**, *111* (9), 3298−3303.

(5) Hertz, H. On the Contact of Elastic Solids. *J. Reine Angew. Math.* **1881**, *92*, 156−171.

(6) Johnson, K.; Kendall, K.; Roberts, A. D. Surface Energy and the Contact of Elastic Solids. *Proc. R. Soc. London. A. Math. Phys. Sci.* **1971**, *324* (1558), 301−313.

(7) Derjaguin, B. V.; Muller, V. M.; Toporov, Y. P. Effect of Contact Deformation on the Adhesion of Elastic Solids. *J. Colloid Interface Sci.* **1975**, *53* (2), 314−326.
(8) Maugis, D. Adhesion of Spheres: The JKR-DMT Transition Using a Dugdale Model. *J. Colloid Interface Sci.* **1992**, *150* (1), 243−269.
(9) Chang, W. R.; Etsion, I.; Bogy, D. B. An Elastic-Plastic Model for the Contact of Rough Surfaces. *J. Tribol.* **1987**, *109* (2), 257−263.
(10) Kogut, L.; Etsion, I. Adhesion in Elastic-Plastic Spherical Microcontact. *J. Colloid Interface Sci.* **2003**, *261* (2), 372−378.
(11) Ma, C. D.; Wang, C.; Acevedo-Vélez, C.; Gellman, S. H.; Abbott, N. L. Modulation of Hydrophobic Interactions by Proximally Immobilized Ions. *Nature* **2015**, *517* (7534), 347−350.
(12) Krieg, M.; Fläschner, G.; Alsteens, D.; Gaub, B. M.; Roos, W. H.; Wuite, G. J. L.; Gaub, H. E.; Gerber, C.; Dufrêne, Y. F.; Müller, D. J. Atomic Force Microscopy-Based Mechanobiology. *Nat. Rev. Phys.* **2019**, *1* (1), 41−57.
(13) Van Engers, C. D.; Cousens, N. E. A.; Babenko, V.; Britton, J.; Zappone, B.; Grobert, N.; Perkin, S. Direct Measurement of the Surface Energy of Graphene. *Nano Lett.* **2017**, *17* (6), 3815−3821.
(14) Johnson, K. L. *Contact Mechanics* **1989**, DOI: 10.1201/b17588-12.
(15) Carpick, R. W.; Ogletree, D. F.; Salmeron, M. A General Equation for Fitting Contact Area and Friction vs Load Measurements. *J. Colloid Interface Sci* . **1999**, *211* (2), 395−400.
(16) Milne, Z. B.; Schall, J. D.; Jacobs, T. D. B.; Harrison, J. A.; Carpick, R. W. Covalent Bonding and Atomic-Level Plasticity Increase Adhesion in Silicon-Diamond Nanocontacts. *ACS Appl. Mater. Interfaces* **2019**, *11* (43), 40734−40748.
(17) Vishnubhotla, S. B.; Chen, R.; Khanal, S. R.; Hu, X.; Martini, A.; Jacobs, T. D. B. Matching Atomistic Simulations and In Situ Experiments to Investigate the Mechanics of Nanoscale Contact. *Tribol. Lett.* **2019**, *67* (3), 1−12.
(18) Liang, J. H.; Milne, Z.; Rouhani, M.; Lin, Y. P.; Bernal, R. A.; Sato, T.; Carpick, R. W.; Jeng, Y. R. Stress-Dependent Adhesion and Sliding-Induced Nanoscale Wear of Diamond-like Carbon Studied Using in Situ TEM Nanoindentation. *Carbon N. Y.* **2022**, *193*, 230−241.
(19) Chen, R.; Vishnubhotla, S. B.; Khanal, S. R.; Jacobs, T. D. B.; Martini, A. Quantifying the Pressure-Dependence of Work of Adhesion in Silicon-Diamond Contacts. *Appl. Phys. Lett.* **2020**, *116* (5), 1−15.
(20) Schall, J. D.; Milne, Z. B.; Carpick, R. W.; Harrison, J. A. Molecular Dynamics Examination of Sliding History-Dependent Adhesion in Si−Si Nanocontacts: Connecting Friction, Wear, Bond Formation, and Interfacial Adhesion. *Tribol. Lett.* **2021**, *69* (2), 1−19.
(21) Li, Z.; Szlufarska, I. Physical Origin of the Mechanochemical Coupling at Interfaces. *Phys. Rev. Lett.* **2021**, *126* (7), 076001.
(22) Raghuraman, S.; Elinski, M. B.; Batteas, J. D.; Felts, J. R. Driving Surface Chemistry at the Nanometer Scale Using Localized Heat and Stress. *Nano Lett.* **2017**, *17* (4), 2111−2117.
(23) Hu, X.; Sundararajan, S.; Martini, A. The Effects of Adhesive Strength and Load on Material Transfer in Nanoscale Wear. *Comput. Mater. Sci.* **2014**, *95*, 464−469.
(24) Harrison, J. A.; White, C. T.; Colton, R. J.; Brenner, D. W. Nanoscale Investigation of Indentation, Adhesion and Fracture of Diamond (111) Surfaces. *Surf. Sci.* **1992**, *271* (1−2), 57−67.
(25) Fujishima, A.; Zhang, X.; Tryk, D. A. Surface Science Reports TiO_2 Photocatalysis and Related Surface. *Phenomena.* **2020**, *63* (2008), 515−582.
(26) Hemmingson, S. L.; Campbell, C. T. Trends in Adhesion Energies of Metal Nanoparticles on Oxide Surfaces: Understanding Support Effects in Catalysis and Nanotechnology. *ACS Nano* **2017**, *11* (2), 1196−1203.
(27) Persson, B. N. J. Nanoadhesion. *Wear* **2003**, *254* (9), 832−834.
(28) Jiang, Y.; Grierson, D. S.; Turner, K. T. Flat Punch Adhesion: Transition from Fracture-Based to Strength-Limited Pull-Off. *J. Phys. D. Appl. Phys.* **2014**, *47* (32), 325301.
(29) Mesarovic, S. D.; Johnson, K. L. Adhesive Contact of Elastic-Plastic Spheres. *J. Mech. Phys. Solids* **2000**, *48* (10), 2009−2033.
(30) Yao, H.; Ciavarella, M.; Gao, H. Adhesion Maps of Spheres Corrected for Strength Limit. *J. Colloid Interface Sci.* **2007**, *315* (2), 786−790.
(31) Long, R.; Hui, C. Y.; Gong, J. P.; Bouchbinder, E. The Fracture of Highly Deformable Soft Materials: A Tale of Two Length Scales. *Annu. Rev. Condens. Matter Phys.* **2021**, *12*, 71−94.
(32) Chen, C.; Wang, Z.; Suo, Z. Flaw Sensitivity of Highly Stretchable Materials. *Extrem. Mech. Lett.* **2017**, *10*, 50−57.
(33) Hui, C. Y.; Glassmaker, N. J.; Tang, T.; Jagota, A. Design of Biomimetic Fibrillar Interfaces: 2. Mechanics of Enhanced Adhesion. *J. R. Soc. Interface* **2004**, *1* (1), 35−48.
(34) Liu, Y.; Gao, Y. Non-Uniform Breaking of Molecular Bonds, Peripheral Morphology and Releasable Adhesion by Elastic Anisotropy in Bio-Adhesive Contacts. *J. R. Soc. Interface* **2015**, *12* (102), 20141042.
(35) Gao, Z.; Gao, Y. Why Do Receptor−Ligand Bonds in Cell Adhesion Cluster into Discrete Focal-Adhesion Sites? *J. Mech. Phys. Solids* **2016**, *95*, 557−574.
(36) Miller, R. E.; Shenoy, V. B. Size-Dependent Elastic Properties of Nanosized Structural Elements. *Nanotechnology* **2000**, *11* (3), 139−147.
(37) Vishnubhotla, S. B.; Chen, R.; Khanal, S. R.; Martini, A.; Jacobs, T. D. B. Understanding Contact between Platinum Nanocontacts at Low Loads: The Effect of Reversible Plasticity. *Nanotechnology* **2019**, *30* (3), 035704.
(38) Jacobs, T. D. B.; Martini, A. Measuring and Understanding Contact Area at the Nanoscale: A Review. *Appl. Mech. Rev.* **2017**, *69* (6), No. 060802.

https://doi.org/10.1021/acs.nanolett.2c02016
Nano Lett. 2022, 22, 5954−5960